Boosting selective hydrogenation through hydrogen spillover on supported-metal catalysts at room temperature

Sai Zhang,[a]* Zhaoming Xia,[b] Mingkai Zhang,[b] Yong Zou,[b] Xiao Chen[b] and Yongquan Qu[a,b]*

[a] School of Chemistry and Chemical Engineering, Northwestern Polytechnic University, Xi'an, 710072, China

[b] Frontier Institute of Science and Technology, Xi'an Jiaotong University, Xi'an, 710049, China

Corresponding Author

* Email: zhangsai1112@nwpu.edu.cn and yongquan@mail.xjtu.edu.cn.

Abstract. Highly efficient hydrogenation of unsaturated substrates with strong absorption on metals at low temperatures is a long-term pursuit. However, due to the scaling relationship of high binding energies on metals, the poor activity and/or selectivity are frequently observed. Herein, we described a strategy of hydrogen spillover to break this scaling relationship to enable highly performed hydrogenation at low temperatures by constructing the dual-active site in supported-metal catalysts. Hydrogen and reactants are selectively activated on metal and the second active sites on support, respectively. Hydrogenation sequentially occurs on the second active sites *via* hydrogen spillover from metal to support. Easy desorption of surface-bounded products substantially re-generates the active sites. Guided by this design, for cinnamaldehyde hydrogenation, PtCo alloys (for H_2 dissociation) supported on hydroxyl-abundant $CoBO_x$ (for aldehyde activation) delivered a high turnover frequency of 2479 h^{-1} (two orders of magnitude over PtCo/C) and 94.5% selectivity of cinnamyl alcohol at room temperature.

1. Introduction

Heterogeneous catalytic reactions under mild conditions, especially at low temperatures, are recognized as energy-efficient synthesis, which are of great promises for practical applications. The ideal scenario for energy-efficient catalysis should satisfy the strong adsorption energy of reactants on catalyst surface for their effective activation through a selective configuration and the relatively weak adsorption of intermediates/products for the re-generation of active sites [1]. However, these are extremely difficult to be realized due to the adsorption energy scaling relationship of various molecules (reactants, intermediates, products) on the catalyst surface [2-5]. Generally, the catalytic activity of a given catalyst with the strong adsorption energies of molecules is poor at low temperatures due to the blocked interfacial active sites by strong adsorption of intermediates and/or products [6]. Although high reaction temperatures can guarantee the thermodynamic desorption of those molecules from the active sites, the accompanied side reactions often lead to the reduced selectivity, especially for reactants with multiple functional groups [7,8]. Thus, to design an energy-efficient catalyst with high activity and selectivity for a specific reaction is highly practical demanded but faces great scientific challenges.

Among various reactions, hydrogenation of unsaturated compounds with strong adsorption on metals is one of the widely adopted processes in chemical industry, which is generally limited by this thermodynamic scaling relationship [2,9-13]. To develop the energy-efficient hydrogenation catalysts, the understandings on the adsorption and activation of substrates and H_2 on catalyst surfaces are pivotal. Fundamentally, H_2 and substrates can be separately activated at different locations in one component or even on different components of supported-metal catalysts [14-22]. Hydrogenation is successfully promoted by a phenomenon called hydrogen spillover (Scheme 1a), which offers an opportunity to break such a thermodynamic scaling relationship and design

the energy-efficient hydrogenation catalyst. In this strategy, metal catalysts with strong binding of chemicals still can activate small size H_2 at low temperatures [23,24]. Design of the second active sites on supports is critical, in which the competitive adsorption of reactants with a specific configuration for the selective activation of targeted functional group should be allowed, and easy desorption of target products to avoid the side reactions and re-expose the active sites. As a result, hydrogenation is achieved through hydrogen spillover from metals to the second active sites.

Guided by this proposal, herein, we construct the dual-active sites in the alloyed PtCo nanoparticles supported on hydroxyl-abundant $CoBO_x$ ($PtCo/CoBO_x$) and demonstrate them as the energy-efficient catalyst to break the scaling limitation and deliver high activity for the selective cinnamaldehyde (CAL)-to-cinnamyl alcohol (COL) hydrogenation at room temperature through a sequential process of (1) H_2 activation on PtCo; (2) hydrogen spillover from PtCo to $CoBO_x$; (3) hydrogenation of the activated CAL on $CoBO_x$ through hydrogen bonding between aldehyde groups of CAL and the interfacial hydroxyls of $CoBO_x$; and (4) easy desorption of the target products of COL on $CoBO_x$ for the re-generation of active sites. Experimental and theoretical investigations suggest that the thermodynamically and kinetically favorable reaction pathway is enabled by hydrogen spillover on the constructed dual-active sites at 25 °C, in comparison with that on metals alone. The catalytic activity of $PtCo/CoBO_x$ is two orders of magnitude higher over that of PtCo alone at 25 °C.

2. Results and Discussion

Catalyst design. Selective hydrogenation of CAL into COL is used as a model reaction to illustrate the concept for the design of energy-efficient supported-metal catalyst at low temperatures. Initially, density functional theory (DFT) calculations were employed to explore

the adsorption behaviors of CAL and COL on Pt surface. Reactant CAL (-2.22 eV) as well as the target product COL (-2.27 eV) show strong binding with Pt surface, leading to a poor catalytic activity of Pt/C at 25 °C (1 *wt.*%, synthesized by chemical coprecipitation method, Figure 1, S1a and S1b). Alloying is a widely proven strategy for improving the catalytic activity of hydrogenation [6,11,18,25]. However, the strong adsorption of CAL (-2.16 eV) and COL (- 2.22 eV) on PtCo still lead to the poor catalytic activity of PtCo/C at 25 °C (1 *wt.*%, Figure 1, S1c and S1d). Significantly promoted hydrogenation activity of supported metals was observed at high temperature of 80 °C. Unfortunately, the non-selective hydrogenation of COL were obtained on both the Pt/C and PtCo/C catalysts, owing to the strong adsorption of CAL and COL on metals and then thermodynamically and kinetically preferred hydrogenation of C=C over C=O as well as the over-hydrogenation (Figure S2), similar as previous reports [7,9,26,27].

Therefore, the grand challenge for selective hydrogenation of CAL into COL at low temperatures lies in the fact of the introduction of the second component to break the limitation of strong adsorption of substrates on metals (Scheme 1a). In this case, the hydrogen bond between hydroxyls of solid and aldehyde of CAL might be a potential binding affinity to control the adsorption configuration of CAL and simultaneously activate the C=O bond. Thereof, $CoBO_x$ with a high surface coverage of hydroxyls is considered as the potential candidate. Theoretically, the stable $CoBO_x(220)$ surface is saturated by six hydroxyls coordinated with two lattice cobalt ions (Scheme S1) [28]. Herein, this $CoBO_x(220)$ surface coverage with six hydroxyls ($CoBO_x$-6OH) was used as the model surface to investigate their interaction with CAL and COL. For CAL, the most stable adsorption configuration on $CoBO_x$-6OH is a tilted one with adsorption energy of -0.38 eV *via* the interaction of –C=O with three surface hydroxyls (Figure 1). In this configuration, the O atom and H atom of –HC=O in CAL bind with two H atoms of two surface

hydroxyls and O atom of another hydroxyl, respectively (Figure S3). The tilted configuration keeps the C=C bond of CAL away from the catalyst surface, theoretically avoiding the hydrogenation of C=C bond. Also, the C=O bond of CAL is elongated from initial 1.230 Å to 1.254 Å, suggesting the effective activation of CAL through the hydrogen bonding for subsequent hydrogenation. While, with the same adsorption configuration of COL on $CoBO_x$-6OH, the adsorption energy of +0.61 eV suggests a thermodynamically unstable adsorption, indicating the easy desorption of COL on $CoBO_x$ (Figure 1 and S4).

Therefore, the DFT calculations reveal that the high surface coverage of hydroxyls on $CoBO_x$ works as the second active site, bringing multiple benefits for the selective hydrogenation of CAL including: (1) providing the sites for CAL adsorption in a tilted configuration to suppress the undesired hydrogenation of C=C bonds, (2) activating the adsorbed aldehyde groups and (3) weakening the COL adsorption to suppress the over-hydrogenation and re-expose the sites.

Based on the above analysis, $PtCo/CoBO_x$ with the constructed dual-active sites of PtCo for H_2 activation and the interfacial hydroxyls of $CoBO_x$ for aldehyde activation is rationally designed as the energy-efficient catalyst to realize the selective CAL-to-COL hydrogenation at 25 °C. Alloyed PtCo nanoparticles are selected as the metal active sites due to their high capability for H_2 activation compared to their individuals [29,30]. Despite the strong adsorption of CAL and COL on PtCo, H_2 still can be activated due to its small size for its accessibility to metal surface. With the concurrence of the successful hydrogen spillover from PtCo to $CoBO_x$, the selective CAL-to-COL hydrogenation could be triggered at 25 °C.

Synthesis and characterizations of $PtCo/CoBO_x$. The $CoBO_x$ nanosheets were synthesized through a chemical reaction between $Co(NO_3)_2$ and $NaBH_4$ under vigorous stirring at room temperature (Figure S5) [28]. Then, the PtCo nanoparticles (6.3 ± 1.4 nm) were successfully

deposited on $CoBO_x$ through a facile wet chemistry process, as observed from the dark field transmission electron microscope (TEM) image (Figure 2a). Electron energy loss spectroscopy (EELS) elemental mappings of $PtCo/CoBO_x$ also confirmed the formation of alloyed PtCo (Figure 2b). The reconstructed fast Fourier transform (FFT) analysis from the high-resolution TEM of PtCo further verified the formation of the alloyed PtCo on $CoBO_x$ (Figure 2c and 2d). The molar ratio of Pt:Co was controlled at 1:1 with a total metal loading of 0.96 *wt.%*, which was determined by combining the inductively coupled plasma (ICP) measurements and energy dispersive spectrometer (EDS) analysis of bimetallic PtCo nanoparticles (Figure S6).

Catalytic performance. As control catalysts, the PtCo nanoparticles with the same weight loading and atom ratio of Pt:Co supported on the carbon black (Figure S1c) and CeO_2 nanorods (Figure S7) were also prepared. The hydrogenation of CAL was performed at 25 °C and 1 MPa H_2. As shown in Figure 3a, $PtCo/CoBO_x$ exhibited a 97.8% conversion of CAL after 9 h. In contrast, only 1.6% and 3.3% conversions of CAL were yielded after 13 h by PtCo/C and $PtCo/CeO_2$, respectively. The turnover frequency (TOF) value based on each exposed surface metal atom of $PtCo/CoBO_x$ (2479 h^{-1}) was 146 and 85 times higher than the values of PtCo/C (17 h^{-1}) and $PtCo/CeO_2$ (29 h^{-1}), respectively (Figure 3b). Therefore, the $PtCo/CoBO_x$ catalyst exhibited the significantly improved catalytic activity at room temperature, suggesting that $PtCo/CoBO_x$ was energy-efficient catalysts herein.

Generally, the enhanced catalytic activity leads to the reduced selectivity of target product [31-33]. Encouragingly, the $PtCo/CoBO_x$ catalyst also delivered a high COL selectivity of 94.5% with only 1.8% of HCAL and 3.7% of HCOL at the end of hydrogenation (Figure 3a). Catalytic stability is also an important criterion to evaluate the performance of $PtCo/CoBO_x$. After the reaction, the $PtCo/CoBO_x$ catalyst was reused for the next cycles by a facile centrifugal

separation process without any other treatments. As shown in Figure 3c, both catalytic activity and selectivity of PtCo/CoBO$_x$ for the CAL-to-COL hydrogenation were preserved for at least 4 cycles at 25 °C. Meanwhile, the characterizations on the spent catalyst demonstrated their structural robustness during hydrogenation (Figure S8). Overall, the PtCo/CoBO$_x$ catalyst exhibited the greatly improved catalytic activity and selectivity as well as the preserved catalytic stability.

Catalytic mechanism. The PtCo/CoBO$_x$ catalyst delivered the dramatically enhanced activity and selectivity for hydrogenation CAL to COL, in comparison with PtCo supported on carbon block and CeO$_2$ nanorods at 25 °C. Previous reports have proved that the electronic structure of metal can greatly affect their catalytic performance of the CAL-to-COL hydrogenation [9,12,34]. As shown in Figure 4a, Pt 4f$_{7/2}$ peak of PtCo/C exhibited the higher binding energy of 71.5 eV than that of PtCo/CeO$_2$ of 71.3 eV as well as that of PtCo/CoBO$_x$ at 71.3 eV, as revealed from the X-ray photoelectron spectroscopy (XPS) analysis. Obviously, the high electronic density of PtCo on CeO$_2$ and CoBO$_x$ resulted in the improved catalytic activity. Although the PtCo/CoBO$_x$ and PtCo/CeO$_2$ catalysts exhibited the similar electronic structures of Pt, their catalytic performances were completely different. Therefore, the superior catalytic performance of PtCo/CoBO$_x$ did not derive from the electronic properties of metals.

Then, to identify the influences of the alloyed PtCo particles, the Pt nanoparticles supported on CoBO$_x$ with 1 *wt.*% loading (Figure S9) were also prepared by the similar synthetic protocol only replacing urea by NaOH. A 98.6% conversion of CAL was yielded after 14 h under 25 °C and 1 MPa H$_2$ (Figure S10). More importantly, Pt/CoBO$_x$ also yielded the 90.1% selectivity of COL. Comparing their catalytic performance, the alloyed PtCo slightly influenced on the hydrogenation activity due to their enhanced capability for H$_2$ activation, while neglectably

impacted on the catalytic selectivity towards COL. Therefore, the comparative results indicated that alloyed PtCo were also not the primary factor for the CAL-to-COL hydrogenation by PtCo/CoBO$_x$.

Hence, the CoBO$_x$ support is expected to play the critical roles in such an energy-efficient hydrogenation. Compared to C and CeO$_2$ supports, the richness of surface hydroxyls in CoBO$_x$ could be confirmed from XPS analysis. As shown in Figure S11, the O 1s peaks at 530.2 eV and 531.5 eV were assigned to the lattice oxygen and surface hydroxyls in CoBO$_x$, respectively. After introducing CAL molecules, the interfacial hydroxyls of solids might provide a potential binding affinity to interact with aldehyde group of CAL for the selective aldehyde activation, according to the DFT calculation in Figure 1. The binding of CAL on CoBO$_x$ was experimentally examined by Fourier-transformed Infrared spectroscopy (FTIR, Figure 3b). Compared to the fresh CoBO$_x$, the new appeared peaks at 1534, 1564 and 715 cm^{-1} for the CAL-treated CoBO$_x$ can be attributed to the characteristic peaks of benzene ring, indicating the presence of CAL on CoBO$_x$. The strong vibration peaks of C=C at 1600 cm^{-1} and weak C=O stretching vibration peak at 1660 cm^{-1} reveal the preferred adsorption/activation *via* aldehyde instead of C=C, thus verifying the tilted adsorption configuration of CAL on CoBO$_x$ [35,36]. While, carbon black and CeO$_2$ nanorods exhibits a very weak interaction with CAL and cannot activate CAL for hydrogenation, evidenced from the unchanged FTIR spectra (Figure S12).

Different from CAL, COL exhibited very weak interaction on CoBO$_x$ from the FTIR analysis (Figure 3b), consistent with DFT calculations (Figure 1). Thus, herein, the kinetically preferred hydrogenation of CAL over COL is anticipated. To confirm this point, hydrogenating a mixture of CAL and COL was performed. Despite the thermodynamically and kinetically favored hydrogenation of C=C [37,38], the hydrogenation of CAL instead of COL was occurred

under 1.0 MPa H_2 at 25 °C (Figure S13). Such a kinetically preferential hydrogenation of CAL into COL could be attributed to the competitive adsorption of CAL on $CoBO_x$ and its effective activation thereby. Thus, both experimental evidences and theoretical calculations demonstrate that $CoBO_x$ with the abundant surface hydroxyl acts as the second sites for the selective adsorption and activation of CAL, avoiding the over-hydrogenation of COL and leading to the improved selectivity.

When PtCo nanoparticles and $CoBO_x$ support were combined, the hydrogenation of CAL could be occurred on their interface of PtCo and $CoBO_x$ or on $CoBO_x$ by the spilled hydrogen. To further examine the reaction pathway, the loading of PtCo nanoparticles on PtCo/$CoBO_x$ was increased to 2 *wt.%* with the preserved molecular ratio of Pt:Co at 1:1 (Figure S14a). The size of PtCo nanoparticles was 6.8 ± 1 nm, similar to that of PtCo/$CoBO_x$ with a total metal loading of 0.96 *wt.%*. In this case, both the exposed PtCo metals and the active sites at the interface of metal and $CoBO_x$ can be approximately considered to be doubled. However, the catalytic activity was only slightly enhanced and the selectivity of COL was well maintained at the same level under the identical reaction conditions (Figure S14b). These results indicated that the metal and interface between PtCo and $CoBO_x$ were not the active sites for the CAL activation and consequent hydrogenation. Comparatively, $CoBO_x$ was indeed the active sites for the CAL activation and sequential hydrogenation.

Therefore, by integrating PtCo and $CoBO_x$ together, the only possible catalytic pathway for CAL hydrogenation is through the spilled hydrogen. The pivotal key to realize the reaction pathway is the effective hydrogen spillover from metal to $CoBO_x$ at low temperatures, which is explored by DFT calculations based on a small PtCo cluster of three Pt and three Co atoms on $CoBO_x$-6OH. When one hydrogen atom (1H) is placed on PtCo, it's stabilized at the bridge site

(Figure 5a). Then, it overcomes a barrier of 0.73 eV to realize hydrogen spillover by migrating to the top site of Pt and then spilling to O atom of $CoBO_x$. Afterwards, the hydrogen migration from one O to adjacent O atom on $CoBO_x$ is very easy with a small energy barrier (0.056 eV). Considering a high H_2 pressure in reactors, PtCo surface is generally covered by a large amount of the activated hydrogen species. When PtCo is covered by six hydrogen (6H), the overall energy barrier of hydrogen spillover is significantly reduced to only 0.29 eV (Figure 5a), consistent with the previous results of the energetically favorable hydrogen spillover from the hydrogen-enriched metals to supports [39]. Thus, the activated hydrogen species can efficiently spill from PtCo to adjacent $CoBO_x$ and then other faraway $CoBO_x$ sites during hydrogenation.

WO$_3$ was used to experimentally confirm the H_2 activation by PtCo/$CoBO_x$ and subsequent hydrogen spillover, in which the activated H species can readily react with the bright yellow WO_3 to form dark blue H_xWO_3 [40,41]. As shown in Figure 5b, the PtCo/$CoBO_x$ catalyst gave the dark blue color of the WO_3 after 1 MPa H_2 treatment at 30 °C. In contrast, WO_3 alone exhibited an almost unchanged color after hydrogen treatment under the same conditions (Figure 5b). Thus, the color evolutions of WO_3 demonstrates that the H_2 activation, dissociation, and hydrogen spillover can successfully occur on the surface of PtCo/$CoBO_x$ catalyst at low temperatures.

The catalytic kinetics were also studied for CAL hydrogenation. As shown in Figure S15-S17, the zero-reaction order characteristic in the initial period was revealed for all three PtCo/$CoBO_x$ PtCo/CeO_2 and PtCo/C catalysts. Then, their reaction rate constants (k) were derived from the slope of the fitting line (Figure S18). This enabled us to extract the activation energy (E_a) by using the Arrhenius equation (Figure 5c). Accordingly, E_a was determined to be 18 kJ mol^{-1} for PtCo/$CoBO_x$, 33 kJ mol^{-1} for PtCo/CeO_2 and 41 kJ mol^{-1} for PtCo/C (Figure 5d).

The lowest E_a of PtCo/CoBO$_x$ suggest the kinetically favorable pathway for the catalytic hydrogenation through the hydrogen-spillover-enabled hydrogenation at room temperature.

Based on the above studies, the reaction pathway was proposed in Scheme 2. Initially, despite the strong adsorption of CAL and COL on PtCo surface, the alloyed metals can still activate small H$_2$ molecule. Meanwhile, the surface abundant hydroxyls on CoBO$_x$ supports serve as the second active sites to selectively activate aldehyde group in CAL through a titled adsorption configuration. Then, the hydrogen spillover of the activated hydrogen species from PtCo to CoBO$_x$ realizes the selective hydrogenation of the activated CAL on supports. COL molecules can be spontaneously desorbed from CoBO$_x$ due to their weak interaction, delivering the high chemoselectivity towards COL. Overall, herein, hydrogen spillover, providing a kinetically favorable pathway and breaking the adsorption energy scaling relationship, boosts catalytic activity and selectivity for CAL-to-COL hydrogenation at room temperature.

3. Conclusion

In summary, we demonstrate a strategy of hydrogen spillover to break the adsorption energy scaling relationship and design the energy-efficient catalysts for the active and selective hydrogenation at room temperature by constructing the dual-active site in supported-metal catalysts. Under this guidance, PtCo/CoBO$_x$ was designed to realize highly active and selective CAL-to-COL hydrogenation at 25 °C through a consequent process of the efficient H$_2$ activation on the alloyed PtCo, hydrogen spillover from PtCo to CoBO$_x$, hydrogenation of the selectively activated aldehyde groups of CAL by the interfacial hydroxyls on CoBO$_x$, and easy desorption of COL for re-exposure of active sites. Experimental and theoretical results unprecedentedly suggest the hydrogen spillover breaks the adsorption limitation and bridges the dual-active sites, offering a thermodynamically and kinetically favorable reaction pathway at low temperatures in

comparison with the hydrogenation on metals alone. Our strategy provides an approach towards the rational design of energy-efficient heterogeneous catalysts that enable efficient and selective reactions under mild conditions.

4. Experimental Details

Synthesis of PtCo/CoBO$_x$, Pt/C, PtCo/C and PtCo/CeO$_2$ catalysts.

Firstly, the CoBO$_x$ nanosheets were synthesized by previous report. Then, 200 mg of as-synthesized CoBO$_x$ nanosheets were dispersed in 50 mL of water through ultrasonication. After adding 3 mg Pt(NH$_3$)$_4$(NO$_3$)$_2$•4H$_2$O, the solution was stirred for 1 h at room temperature. Subsequently, the reaction temperature was increased to 75 °C after adding 15 mL of aqueous urea solution (10 mg mL^{-1}) for another 2 h. After cool to room temperature, 5 mL of the ice-cold fresh aqueous NaBH$_4$ solution (1 mg mL^{-1}) was added. Finally, the PtCo/CoBO$_x$ catalysts were thoroughly washed by distilled water for three times and collected by centrifugation.

The Pt/C and PtCo/C catalysts with 1 *wt*% of metal loading were synthesized with the same process of PtCo/CoBO$_x$. The atom ratio of Pt and Co was controlled to 1:1 for the PtCo/C catalysts.

The CeO$_2$ nanorods was synthesized by hydrothermal process. Ce(NO$_3$)$_3$·6H$_2$O (1.736 g) and NaOH (19.2 g) were dissolved in 10 mL and 70 mL of MQ water, respectively. After aging at room temperature for 30 min, the mixture was transferred into a stainless steel autoclave for hydrothermal treatment at 100 °C for 24 h. The products were collected by centrifugation, washed with copious amount of water, and dried at 60 °C.

The PtCo/CeO$_2$ catalysts with 1 wt% of metal loading and 1:1 atom ratio of Pt:Co were synthesized with the same process of PtCo/CoBO$_x$.

Characterizations.

Transmission electron microscope (TEM) studies were conducted with a Hitachi HT-7700 transmission electron microscope with an accelerating voltage of 120 kV. X-ray photoelectron spectroscopy (XPS) spectra was acquired using a Thermo Electron Model K-Alpha with Al K_α as the excitation source. Fourier-transformed Infrared spectroscopy (FTIR) analysis was performed by using a Bruker Vertex 80 with KBr pellet. Electron energy loss spectroscopy (EELS) and high-resolution TEM were conducted on a Titan Cubed Themis G2 300 (FEI) aberration-corrected scanning transmission electron microscope.

Catalytic Hydrogenation.

The hydrogenation of CAL was carried out in a stainless-steel autoclave equipped with the pressure control system. For a typical catalytic reaction, 1 mmol of CAL and 5 mg of catalysts were added in 2 mL of isopropanol. The reactions were performed in the autoclave charged with 1 MPa H_2 at 25 °C. Finally, the products were analyzed by gas chromatography-mass spectrometer (GC-MS) and GC.

Supporting Information.

This file provides more detailed information regarding DFT calculations, TEM image and catalytic performance of Pt/C and PtCo/C catalysts, adsorption configurations of CAL and COL on the surface of CoBO$_x$-6OH, EDS analysis of PtCo/CoBO$_x$, TEM image of the used PtCo/CoBO$_x$ catalyst, TEM and HRTEM images of Pt/CoBO$_x$, catalytic performance of Pt/CoBO$_x$ for the CAL hydrogenation, FTIR spectra of CeO$_2$ and carbon before and after the CAL/COL treatments, catalytic activity of PtCo/CoBO$_x$ for COL hydrogenation in the presence of CAL, TEM image and catalytic performance of PtCo/CoBO$_x$ for the CAL hydrogenation, kinetic analysis.

Acknowledgment

References

1. Medford AJ, Vojvodic A, Hummelshøj JS, et al. From the Sabatier principle to a predictive theory of transition-metal heterogeneous catalysis. *J. Catal.* 2015;328:36-42.

2. Studt F, Abild-Pedersen F, Bligaard T, Sørensen RZ, Christensen CH, Nørskov JK. Identification of non-precious metal alloy catalysts for selective hydrogenation of acetylene. *Science.* 2008;320:1320-1322.

3. Khorshidi A, Violet J, Hashemi J, Peterson AA. How strain can break the scaling relations of catalysis. *Nat. Catal.* 2018;1:263-268.

4. Sun G, Zhao Z-J, Mu R, et al. Breaking the scaling relationship via thermally stable Pt/Cu single atom alloys for catalytic dehydrogenation. *Nat. Commun.* 2018;9:4454.

5. Qin R, Zhou L, Liu P, et al. Alkali ions secure hydrides for catalytic hydrogenation. *Nat. Catal.* 2020;3:703-709.

6. Zhang L, Zhou M, Wang A, Zhang T. Selective hydrogenation over supported metal catalysts: From nanoparticles to single Atoms. *Chem. Rev.* 2020;120:683-733.

7. Ide MS, Hao B, Neurock M, Davis RJ. Mechanistic insights on the hydrogenation of α,β-Unsaturated ketones and aldehydes to unsaturated alcohols over metal catalysts. *ACS Catal.* 2012;2:671-683.

8. Yang Y, Rao D, Chen Y, et al. Selective hydrogenation of cinnamaldehyde over Co-based intermetallic compounds derived from layered double hydroxides. *ACS Catal.* 2018;8:11749-11760.

9. Lan X, Wang T. Highly selective catalysts for the hydrogenation of unsaturated aldehydes: A review. *ACS Catal.* 2020;10:2764-2790.

10. Schauermann S. Partial hydrogenation of unsaturated carbonyl compounds: Toward ligand-directed heterogeneous catalysis. *J. Phys. Chem. Lett.* 2018;9:5555-5566.

11. Luneau M, Lim JS, Patel DA, Sykes ECH, Friend CM, Sautet P. Guidelines to achieving high selectivity for the hydrogenation of alpha,beta-unsaturated aldehydes with bimetallic and dilute alloy catalysts: A review. *Chem. Rev.* 2020:doi: 10.1021/acs.chemrev.1020c00582.

12. Wang X, Liang X, Geng P, Li Q. Recent advances in selective hydrogenation of cinnamaldehyde over supported metal-based catalysts. *ACS Catal.* 2020;10:2395-2412.

13. Niu Z, Zhang W, Lan PC, Aguila B, Ma S. Promoting frustrated Lewis pairs for heterogeneous chemoselective hydrogenation via the tailored pore environment within metal-organic frameworks. *Angew. Chem. Int. Ed.* 2019;58:7420-7424.

14. Zaera F. The long and winding road to catalysis. *Nature.* 2017;541:37-38.

15. Jiang L, Liu K, Hung SF, et al. Facet engineering accelerates spillover hydrogenation on highly diluted metal nanocatalysts. *Nat. Nanotechnol.* 2020:doi.org/10.1038/s41565-41020-40746-x.

16. Marcinkowski MD, Jewell AD, Stamatakis M, et al. Controlling a spillover pathway with the molecular cork effect. *Nat. Mater.* 2013;12:523-528.

17. Wang S, Zhao ZJ, Chang X, et al. Activation and spillover of hydrogen on sub-1 nm palladium nanoclusters confined within sodalite zeolite for the semi-hydrogenation of alkynes. *Angew. Chem. Int. Ed.* 2019;58:7668-7672.

18. Giannakakis G, Flytzani-Stephanopoulos M, Sykes ECH. Single-atom alloys as a reductionist approach to the rational design of heterogeneous catalysts. *Acc. Chem. Res.* 2019;52:237-247.

19. Wu Q, Zhang C, Arai M, et al. Pt/TiH$_2$ catalyst for ionic hydrogenation via stored hydrides in the presence of gaseous H$_2$. *ACS Catal.* 2019;9:6425-6434.

20. Cao Y, Chen B, Guerrero-Sánchez J, et al. Controlling selectivity in unsaturated aldehyde hydrogenation using single-site alloy catalysts. *ACS Catal.* 2019;9:9150-9157.

21. Zhang J, Gao Z, Wang S, et al. Origin of synergistic effects in bicomponent cobalt oxide-platinum catalysts for selective hydrogenation reaction. *Nat. Commun.* 2019;10:4166.

22. Wei J, Qin SN, Liu JL, et al. In situ Raman monitoring and manipulating of interfacial hydrogen spillover by precise fabrication of Au/TiO$_2$/Pt sandwich structures. *Angew. Chem. Int. Ed.* 2020;59:10343-10347.

23. Kaeffer N, Mance D, Coperet C. N-Heterocyclic carbene coordination to surface copper sites in selective semihydrogenation catalysts from solid-state NMR spectroscopy. *Angew. Chem. Int. Ed.* 2020;59:doi:10.1002/anie.202006209.

24. Liu P, Qin R, Fu G, Zheng N. Surface coordination chemistry of metal nanomaterials. *J. Am. Chem. Soc.* 2017;139:2122-2131.

25. Lv Y, Han M, Gong W, et al. Fe-Co alloyed nanoparticles catalyzing efficient hydrogenation of cinnamaldehyde to cinnamyl alcohol in water. *Angew. Chem. Int. Ed.* 2020;59:doi: 10.1002/anie.202009913.

26. Zhao M, Yuan K, Wang Y, et al. Metal-organic frameworks as selectivity regulators for hydrogenation reactions. *Nature.* 2016;539:76-80.

27. Weng Z, Zaera F. Sub-monolayer control of mixed-oxide support composition in catalysts via atomic layer deposition: Selective hydrogenation of cinnamaldehyde promoted by (SiO$_2$-ALD)-Pt/Al$_2$O$_3$. *ACS Catal.* 2018;8:8513-8524.

28. Zhang S, Huang Z, Chen X, et al. Hydrogen activation enabled by the interfacial frustrated Lewis pairs on cobalt borate nanosheets. *J. Catal.* 2019;372:142-150.

29. Kyriakou G, Boucher MB, Jewell AD, et al. Isolated metal atom geometries as a strategy for selective heterogeneous hydrogenations. *Science.* 2012;335:1209-1212.

30. Tsang SC, Cailuo N, Oduro W, et al. Engineering preformed cobalt-doped platinum nanocatalysts for ultraselective hydrogenation. *ACS Nano.* 2008;2:2547-2553.

31. Wu B, Huang H, Yang J, Zheng N, Fu G. Selective hydrogenation of alpha,beta-unsaturated aldehydes catalyzed by amine-capped platinum-cobalt nanocrystals. *Angew. Chem. Int. Ed.* 2012;51:3440-3443.

32. Kahsar KR, Schwartz DK, Medlin JW. Control of metal catalyst selectivity through specific noncovalent molecular interactions. *J. Am. Chem. Soc.* Jan 8 2014;136:520-526.

33. Shimizu K-i, Miyamoto Y, Kawasaki T, Tanji T, Tai Y, Satsuma A. Chemoselective Hydrogenation of Nitroaromatics by Supported Gold Catalysts: Mechanistic Reasons of Size- and Support-Dependent Activity and Selectivity. *J. Phys. Chem. C.* 2009;113:17803-17810.

34. Koh K, Sanyal U, Lee MS, et al. Electrochemically tunable proton-coupled electron transfer in Pd-catalyzed benzaldehyde hydrogenation. *Angew. Chem. Int. Ed.* 2020;59:1501-1505.

35. Kahsar KR, Schwartz DK, Medlin JW. Control of metal catalyst selectivity through specific noncovalent molecular interactions. *J. Am. Chem. Soc.* 2013;136:520-526.

36. Wang H, Bai S, Pi Y, Shao Q, Tan Y, Huang X. A strongly coupled ultrasmall Pt_3Co nanoparticle-ultrathin $Co(OH)_2$ nanosheet architecture enhances selective hydrogenation of α,β-unsaturated aldehydes. *ACS Catal.* 2018;9:154-159.

37. Zhao M, Yuan K, Wang Y, et al. Metal–organic frameworks as selectivity regulators for hydrogenation reactions. *Nature.* 2016;539:76-80.

38. Cao X-M, Burch R, Hardacre C, Hu P. Reaction mechanisms of crotonaldehyde hydrogenation on Pt(111): Density functional theory and microkinetic modeling. *J. Phys. Chem. C.* 2011;115:19819-19827.

39. Karim W, Spreafico C, Kleibert A, et al. Catalyst support effects on hydrogen spillover. *Nature.* 2017;541:68-71.

40. Wang C, Guan E, Wang L, et al. Product selectivity controlled by nanoporous environments in zeolite crystals enveloping rhodium nanoparticle catalysts for CO_2 hydrogenation. *J. Am. Chem. Soc.* 2019;141:8482-8488.

41. Khoobiar S. Particle to particle migration of hydrogen atoms on platinum—alumina catalysts from particle to neighboring particles. *J. Phys. Chem.* 1964;68:411-412.
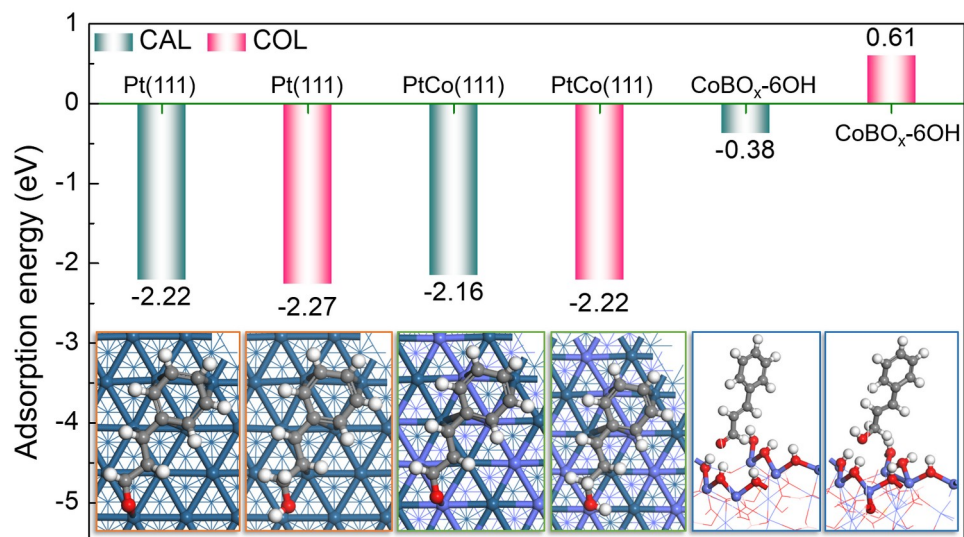
Figure 1. Adsorption energies and configurations of CAL and COL on Pt(111), PtCo(111) and CoBO$_x$-6OH surfaces.
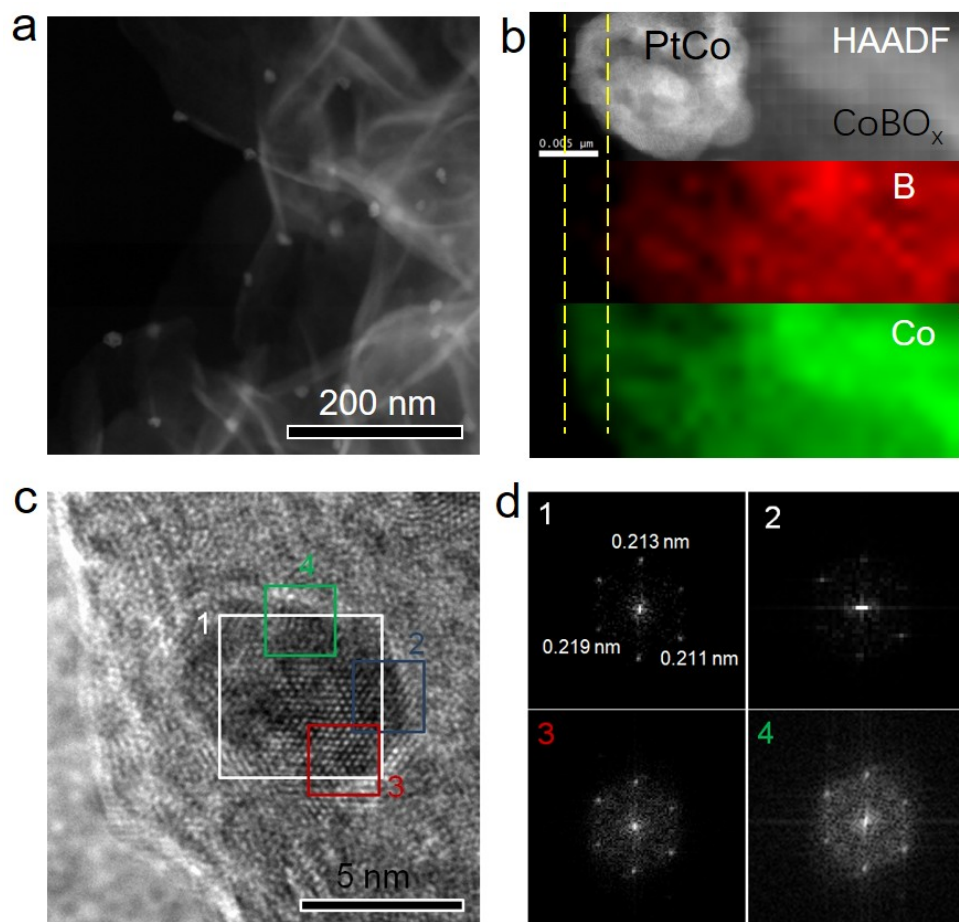
Figure 2. Structural characterizations of the PtCo/CoBO$_x$ catalysts. (a) Dark field TEM image, (b) EELS mappings, (c) high resolution TEM image and (d) FFT analysis of the alloyed PtCo nanoparticles.
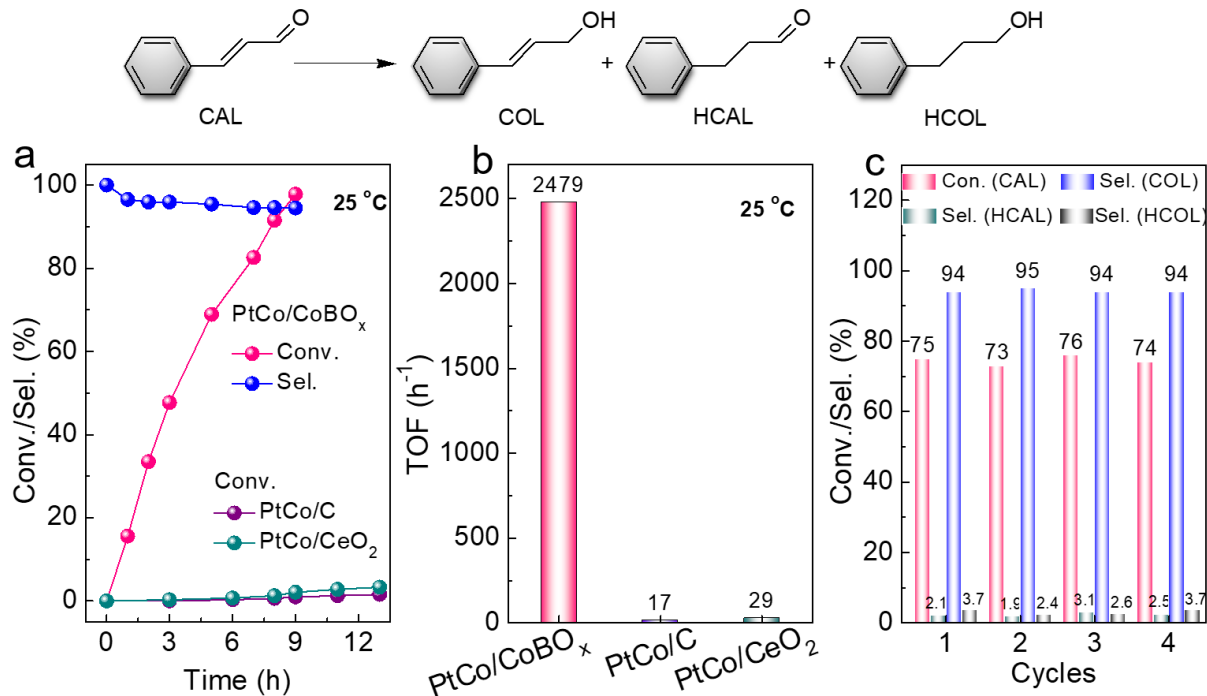
Figure 3. (a) Catalytic performance and (b) TOF values of the CAL hydrogenation. TOF was defined as the number in moles of the converted CAL on the exposed metal atoms in moles per hour. (c) Catalytic stability of PtCo/CoBO$_x$. **Reaction conditions:** CAL (1.0 mmol), IPA (2.0 mL), catalysts (5.0 mg), 1.0 MPa H$_2$, 25 °C and 8.0 h.
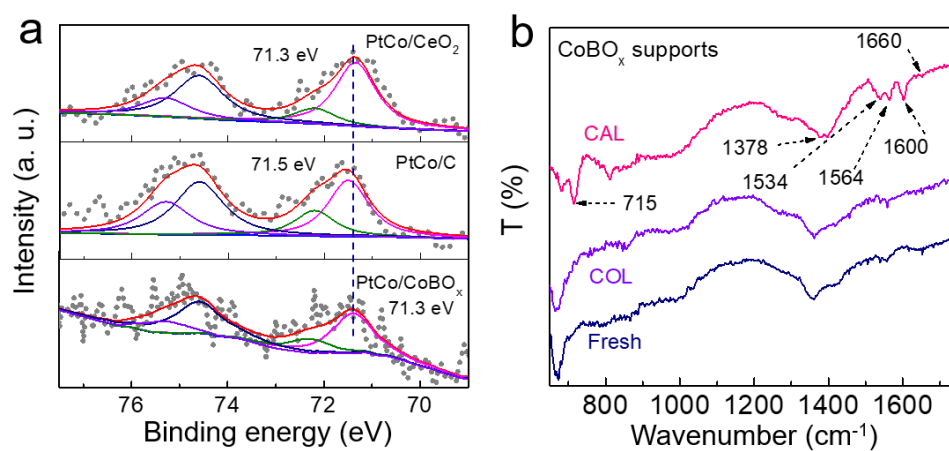
Figure 4. (a) XPS analysis of various PtCo catalysts. (b) FTIR spectra of CoBO$_x$ before and after CAL/COL treatments.
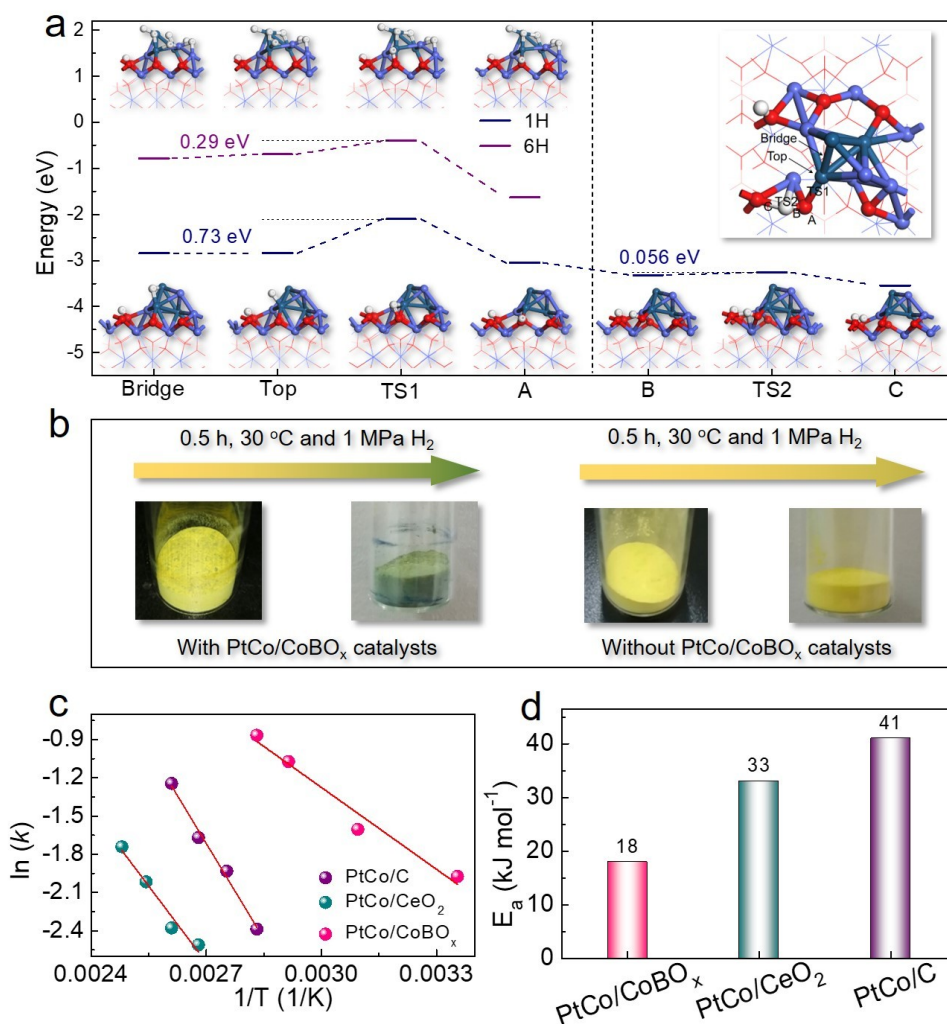
Figure 5. (a) Hydrogen spillover process from PtCo to CoBO$_x$. Dark green, blue, red and gray are representative of Pt, Co, O and H atom, respectively. (b) Photographs of samples of 1 g of WO$_3$ mixed with and without 0.04 g PtCo/CoBO$_x$ after treatment with 1 MPa H$_2$ at 30 °C for 0.5 h. (c) Plot of ln k as a function of ($1/T$) for various catalysts, derived from CAL reaction rates *vs* reaction time. (d) E_a of various catalysts for the CAL hydrogenation.
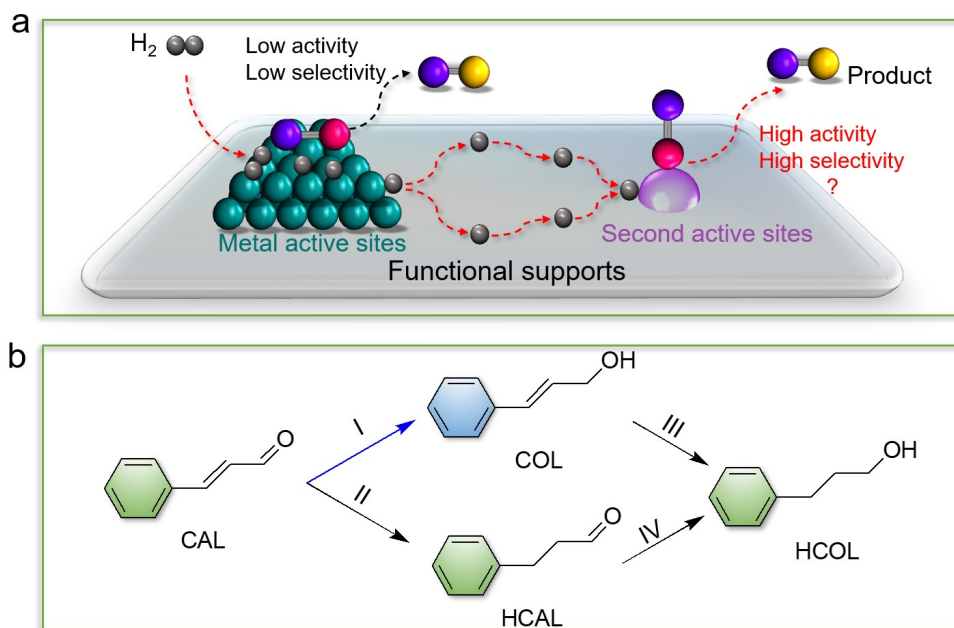
Scheme 1. (a) Proposed hydrogenation pathway on dual active sites enabled by hydrogen spillover. (b) Reaction steps of the CAL hydrogenation.
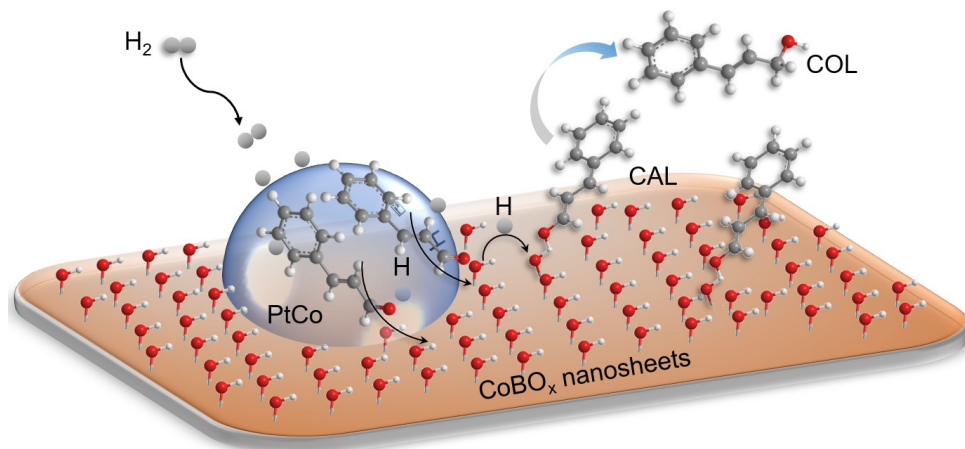
Scheme 2. Hydrogen spillover of dual-active sites for breaking adsorption scaling relationship and enabling the selective hydrogenation of CAL into COL. Blue, red, light gray and dark gray are representative of PtCo nanoparticles, O atom, H atom and C atom, respectively.